2013

Particle Cluster Size Distribution in Gas–Solid Downer Units

A. Lanza
The University of Western Ontario, Canada

M.A. Islam
The University of Western Ontario, Canada

H. de Lasa
The University of Western Ontario, Canada

PARTICLE CLUSTER SIZE DISTRIBUTION IN GAS–SOLID DOWNER UNITS

A. Lanza, M.A. Islam, H. de Lasa*
Chemical Reactor Engineering Centre, Faculty of Engineering,
The University of Western Ontario, 1151 Richmond Street,
London, Ontario, Canada, N6A 5B9
*T: 519-661-2144, F: 519-850-2931, E: hdelasa@eng.uwo.ca

ABSTRACT

This work establishes individual particle cluster size distributions in gas-solid downflow reactors. To accomplish this, local cluster particle characteristics are determined using a significantly enhanced data analysis. Data reported corresponds to experiments carried out in a circulating fluidized bed downer cold model unit of 3.0 m height and 0.0257 m internal diameter. The solid used was a fluid catalytic cracking (FCC) catalyst with a mean particle diameter of 84.42 μm and a particle density of 1,722 kg/m^3. The superficial gas velocity and solid mass fluxes were varied from 1.0 to 2.5 m/s and from 10 to 106 kg/m^2·s, respectively. It is proven that for all conditions and radial positions considered, cluster particle size distributions are consistently asymmetric, with cluster sizes varying from 1 to 9 average size particles, and with the smaller clusters being the most abundant.

1. INTRODUCTION

Downflow reactors have been recently utilized in industrial applications because they do not display the particle back mixing as observed in upflow units. They have: (a) a much more uniform gas-solid flow pattern, (b) shorter contact times, (c) reduced axial dispersion, (d) the capability of handling higher solids/gas load ratios, and (e) the possibility to operate at higher temperatures; as demonstrated by J.X. Zhu ([1]) and Z. Wang ([2]). As an example, downer reactors provide a valuable reactor configuration for fluid catalytic cracking (FCC). With this alternative, the optimization of FCC is mainly related to the control of catalyst/oil contact times with the goal of increasing gasoline productivity as well as decreasing dry gas and coke.

To achieve this, a CREC-GS-Optiprobe equipped with a Graded Refractive Index (GRIN) lens is used. The signal data baseline is set using a rigorous methodology. It is proposed that the position of the baseline be selected for every downer level and operational condition in compliance with solid flow mass balances. Using this approach, the noise resulting from secondary reflections is cancelled and all valuable data is kept in the time series.

In order to analyze the train of optiprobe signals, it is required to set signal baselines. Each signal baseline is defined in the present study as, $X+n·σ_x$, where X is the signal average; $σ_x$ is the signal standard deviation; and n is a baseline reference factor. The important influence of the "n" parameter on signal analysis is noticeable; therefore, it is advisable to set a signal baseline as high as possible. This is significant in order to

avoid secondary particle reflections or noise contributions. However, the higher the baseline, the larger the loss of relevant cluster data. Thus, the definition of the "*n*" parameter is critical and requires an optimization approach. A detailed explanation on how to set the baseline is reported in this manuscript.

2. EXPERIMENTAL SETUP AND METHODS

2.1 Experimental setup

The experimental riser-downer unit used in this research was made of transparent acrylic tubes; the internal diameter of both riser and downer is 0.0254 cm. The downer section of the equipment was used to study the hydrodynamics of the gas-solid flow. The solid phase consisted of FCC particles which had the same characteristics as those employed by M.A. Islam et al ([3]). These had a mean particle diameter of 84.42 μm with a standard deviation of 33.62 μm, and an apparent particle density of 1,722 kg/m^3. The fluidization gas was air at room pressure and temperature conditions. The solid mass flux and superficial gas velocity were varied from 10 to 106 kg/m^2·s and from 1.0 to 2.5 m/s respectively. A detailed explanation regarding the design of this unit is reported in S. Nova et al ([4]), ([5]) and ([6]).

2.2 CREC-GS-Optiprobes

The data used to estimate fluid dynamic properties in the downer unit was acquired with the CREC-GS-Optiprobes developed at The University of Western Ontario. Two CREC-GS-Optiprobes were placed at a 1.85 m height in the downer below the injection port, and were separated axially by 0.006 m. It was considered that at 1.60 m, the particles reached terminal velocity. A confirmation of the fully developed flow pattern (clusters evolving at terminal velocity), as shown via the pressure drop along the downer, is provided in Islam et al ([3]). This optic sensor belongs to the class of fibre optic reflective sensors. The total typical recording signal period in each one of the CREC-GS-Optiprobes was set to 1 s or 100,000 data points. At least 5 signal trains of 1 s, or 500,000 data points, were recorded at every radial position and for each operating condition.

2.3 Baseline reference

A new methodology for setting the data baseline using solid mass balances is adopted in the present study. A sample of the time signals recorded by both the upper and lower probes is reported in Fig. 1. The vertical axis of Fig.1 reports the signal time series expressed in volts; likewise, the horizontal axis represents time in seconds. For a clear illustration of the signals, this graph reports only 0.005 s of signal duration, as recorded by CREC-GS-Optiprobes at the radial position of r/R = 0.1. One can notice that there is a delay time between both signals which represents the time shift between the upper to the lower optiprobes. This is the time displacement required for the particle cluster to move from one detection volume to the other. For the conditions of Fig. 1, the time displacement is 0.0022 s. This time displacement is estimated using a cross-correlation function as explained by A. Lanza et al ([7])

In order to analyze optiprobe signals, as it was mentioned in the introduction, it is required to set signal baselines. With this goal in mind, each signal baseline was defined in the present study as,
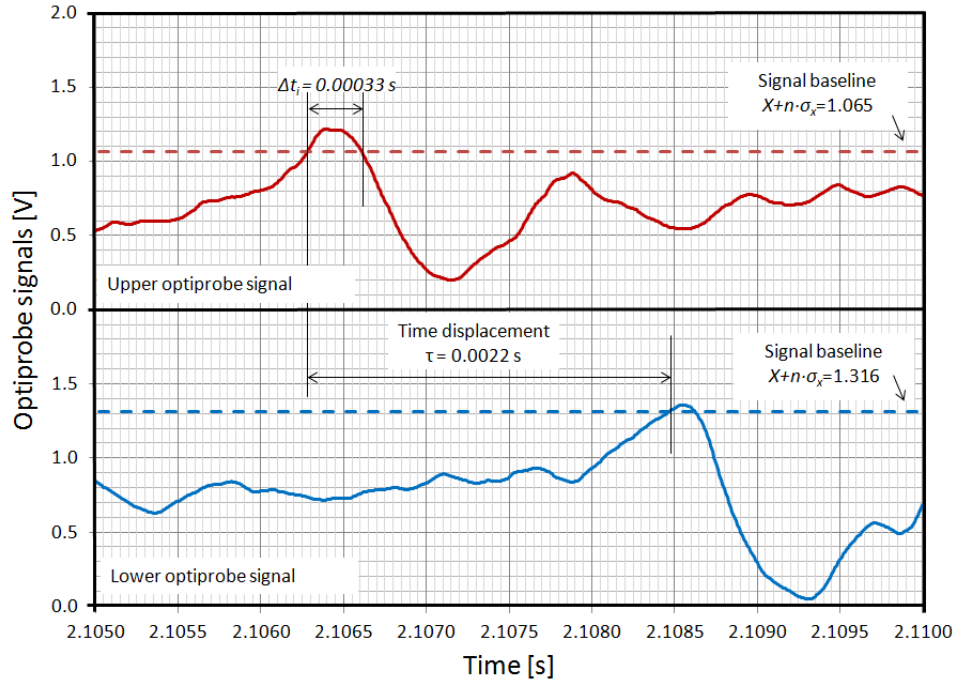
$$X + n \cdot \sigma_x \tag{1}$$

Fig. 1. CREC-GS-Optiprobe signals with description of baseline levels

The strong influence of n on signal analysis has been reported in the literature by several researchers, e.g.: Manyele et al (8), Soong et al (9), and Sharma et al (10). However, there is not relevant information reported in the literature regarding to how to set the baseline rigorously. Fig. 1 also describes an example of selected baselines. As one can notice, it is advisable to set a signal baseline as high as possible to avoid secondary particle reflections or noise contributions. However, the higher the baseline, the larger the loss of relevant cluster data information.

On the other hand, in the present study, a rigorous methodology was used for setting the signal baseline. For this purpose, instead of using an arbitrary and fixed level definition, the baseline was chosen at every downer level and at every operational condition in compliance with solid mass balances as shown in Eq. (2):

$$G_s = \frac{\rho_p}{A} \int_0^A u_s \varepsilon_s dA \qquad (2)$$

where: G_s is the cross-sectional solid mass flux; ρ_p is the particle density; A is the total internal area of the downer reactor; u_s is the time weighted average radial cluster velocity; and ε_s is the time average radial solid concentration.

Using this approach, noise resulting from secondary reflections is eliminated and all valuable data is kept in the time series. A total of 9 operational conditions were considered. Results regarding the baseline reference factor are shown in Table 1. It is important to notice that a close value of the n baseline reference factor was obtained for both, the upper and the lower optiprobes, which provides strong evidence of the relation between both signals.

From Table 1, one can notice that the solid mass flux, *Gs*, has a very significant influence on the *n* baseline reference factor, while the superficial gas velocity, *Usg*, does not. To explain this behavior of *n* with G_s changes, one can argue that a larger G_s leads to more significant secondary ray reflections from particles or particle clusters increasing both the signal average, *X*, and the standard deviation σ_x.

Table 1. Baseline reference factor experimental results

Operational conditions	Solid mass flux (Gs, kg/m²/s)	Superfitial gas velocity (Usg, m/s)	Upper optiprobe baseline reference factor, *n*	Lower optiprobe baseline reference factor, *n*
1	9.8	0.9	3.5	3.5
2	15.1	1.4	3.3	3.3
3	49.9	1.2	1.7	1.9
4	56.6	1.9	2.5	2.5
5	64.7	1.2	1.9	2.0
6	76.3	2.5	1.9	2.2
7	82.1	1.7	2.0	2.1
8	91.2	2.5	1.6	2.0
9	105.8	1.2	1.6	1.5

Thus, to set an example of the baseline calculation, for the upper optiprobe signal described in Fig. 1, $n = 2.087$, $X = 0.684$ V, and $\sigma_x = 0.182$ V. As a result, the *n* baseline reference factor can be estimated as: $X + n \cdot \sigma_x = 0.684 + 2.087 \cdot 0.182 = 1.065\ V$. In this respect, it is important to mention that for each operational condition, a proper baseline reference factor has to be found. This is given the *n* parameter dependence on the solid mass flux.

3. PARTICLE CLUSTER SIZE DISTRIBUTION RESULTS

To determine cluster sizes, the string cluster configuration proposed by Krol et al ([11]) was assumed as applicable in the present study. Thus, we can assume that particles agglomerate on the basis of a number of leading particles, which are followed by a number of trailing particles. This vertical chain of *N* number of particles in contact with each other is a hydrodynamically favored cluster shape. This favored cluster shape offers a configuration where drag forces are minimized. Therefore, the cluster shape is assumed to be a vertical chain of *N* number of spherical particles in contact with each other. The numbers of particles in each one of these clusters can be estimated according to the Eq. (3) as follows,

$$N_i = \frac{(u_{si}\Delta t_i) - h + d_p}{d_p} \tag{3}$$

where u_{si} represents the terminal velocity of the cluster *i*, at the corresponding pair of time series; *Δtᵢ* is the time that cluster *i* needs to move down into the sensing region of the upper optiprobe; *h* is the characteristic transversal dimension of the optiprobe sensing region (focal point); and d_p is the particle diameter; S. Nova et al ([5]).

Therefore, to estimate a cluster size, it is necessary to first determine the cluster velocity u_s, with Eq. (4),

$$u_{si} = \frac{d}{\tau_i} \tag{4}$$

where *d* is the distance between the upper and lower focal sensor regions; and τ_i represents the time shift or time displacement between both signals for the cluster *i*.

Once the time shift is obtained via signal cross-correlation, as proposed by A. Lanza et al (7), and given that the spacing *d* between the upper and lower focal regions equals 0.006 m, the cluster velocity can be calculated. In the case of Fig. 1, the time displacement is 0.0022 s. The cluster velocity, U_{si}, can, thus, be determined to be 2.73 m/s. Therefore, for the upper optiprobe signal (Fig. 1), the number of particles can be estimated as:

$$N_i = \frac{(u_{si}\Delta t_i) - h + d_p}{d_p} = \frac{\left(2.73\frac{m}{s}\right)(0.0003\ s) - (118 \cdot 10^{-6}\ m) + (84.42 \cdot 10^{-6}\ m)}{(84.42 \cdot 10^{-6}\ m)}$$
$$= 9.29 \approx 9 \text{ particles}$$

Given that for every cluster in a size distribution, the calculated particle number is most likely to be a decimal number, one can approximate the size of every cluster using the closest integer class.

Table 2 summarizes the total number of clusters studied at the various operating conditions of the present study. One can notice that more than 17,000 clusters were considered. Information obtained at 10 radial positions was used for calculations. The downer tube cross-section was divided into 10 concentric annuli and the solid mass flux, *Gs*, was determined in each circular strip of cross-section area as proposed by X.B. Qi et al (12). It was judged that these data in conjunction with the enhanced data analysis, provide an adequate evaluation of the local averaged solid concentration at various radial downer positions.

Table 2. Operating conditions and number of clusters studied

Operational conditions	Solid mass flux (Gs, kg/m^2/s)	Superfitial gas velocity (Usg, m/s)	Number of cluster studied
1	9.8	0.9	899
2	15.1	1.4	1209
3	49.9	1.2	1355
4	56.6	1.9	1675
5	64.7	1.2	2823
6	76.3	2.5	1442
7	82.1	1.7	2444
8	91.2	2.5	2143
9	105.8	1.2	3272

On the other hand, Fig. 2 describes the observed individual particle cluster size distributions. In this figure, the total number of clusters observed for each operational condition in the complete downer cross-sectional area is reported. The vertical axis of Fig. 2 reports particle cluster size distributions on a percentual basis while the horizontal axis reports the operational conditions studied (e.g. solid mass flux, G_s, and cluster slip velocities, U_{gs}). The side legend in Fig. 2 describes the cluster sizes established as a number of 84.42 μm average particles: from 1 to 10 average particle sizes.

It can be noticed in Fig. 2 that, for a given operational condition and cluster population, the cluster size distribution is asymmetric with smaller particle clusters being more dominant than larger clusters. Fig. 3 reports a zoom of the $G_s = 91.2$ kg/m^2/s, and $U_{sg} = 2.5$ m/s condition where more than 28% of clusters have only one particle. Moreover, the sum of all clusters with an N value larger

than 6 is, in this case, smaller than 15%. These strongly asymmetric distributions of cluster size and cluster slip velocity were found to be a characteristic cluster feature for all operating conditions considered in the present study. This means that clusters with a large number of particles are less likely to survive. One can argue that this behavior is the result of the collision between clusters, with this collision tending to break larger clusters in smaller ones.
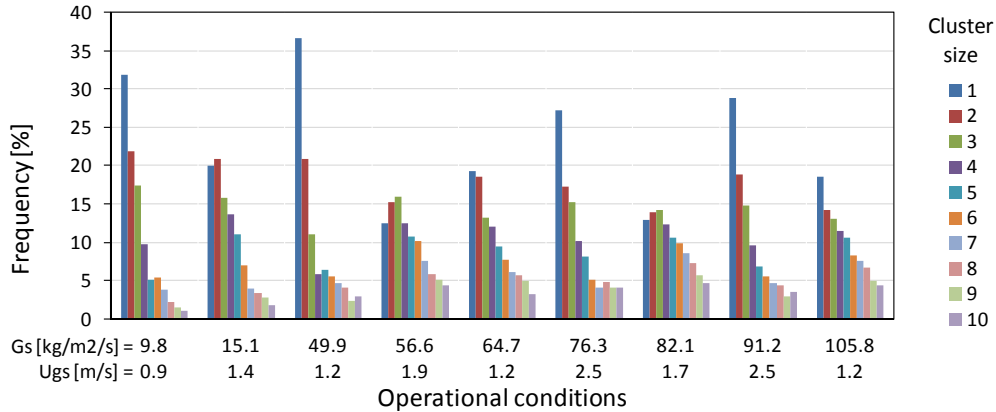

Fig. 2. Individual particle cluster size distributions at various solid fluxes and gas velocities
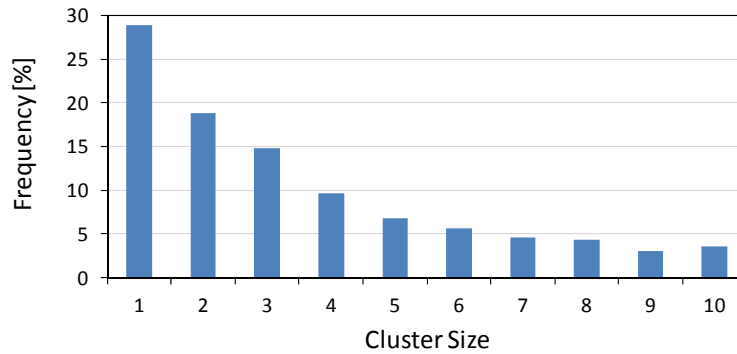

Fig. 3. Distribution of the number of particles in clusters for Usg = 2.5 m/s, Gs = 91.2 kg/m^2/s

Fig.4 provides a weighted average of individual particle cluster size distributions for the complete set of operational conditions. The error bars represent the weighted standard deviation. As a result, one can conclude that for all operational conditions considered, the cluster size distributions are asymmetric with smaller particle clusters being more dominant than larger particle clusters.
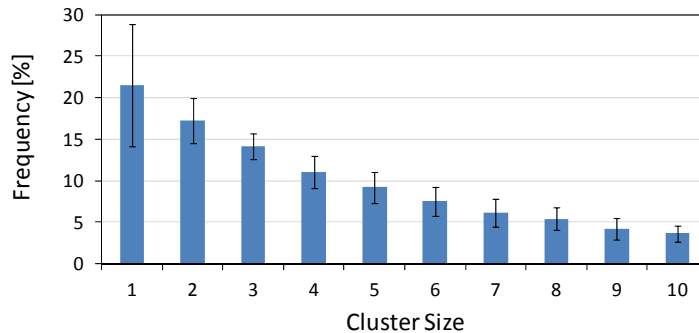

Fig. 4. Individual particle cluster size distribution averages

To gain a better understanding of the particle cluster size distributions in downers reactors, the radial position influence on cluster size distribution was also considered. Fig. 5 reports cluster size distribution changes with radial positions having r/R = 0 as the column center and r/R = 1 as the internal downer wall, the legend in this figure describes cluster sizes established on the basis of the number of average particle sizes (e.g. from 1 to 10). Values of the distributions reported in Fig. 5, correspond to weighted average distributions with error bars representing weighted standard deviations.
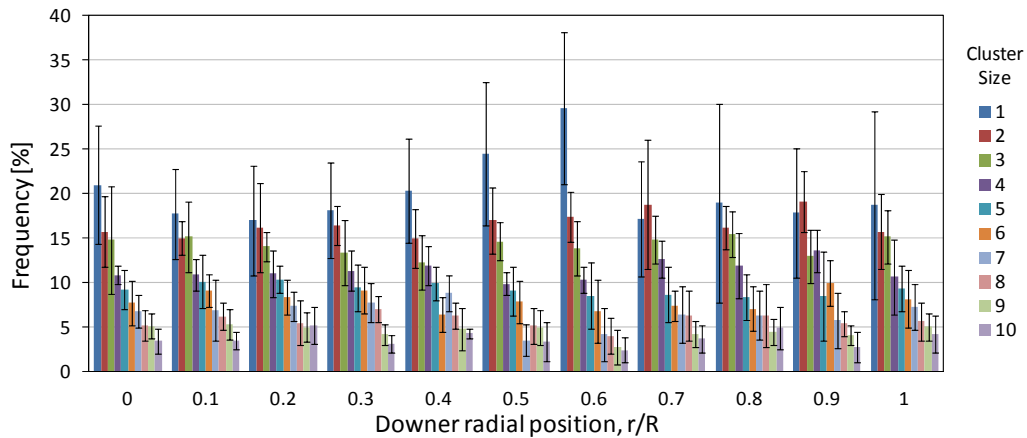

Fig. 5. Individual particle cluster size distribution weighted averages for all operational conditions studied

Fig. 6 reports a zoom of the individual cluster size distribution weighted averages at r/R=0 in Fig. 5. One can notice that the cluster size distributions in downers are in agreement with the total average distributions as described in Fig. 4. This provides confirmation that it is more likely to find clusters in a downer with just a few particles, than to find clusters with a large number of particles.
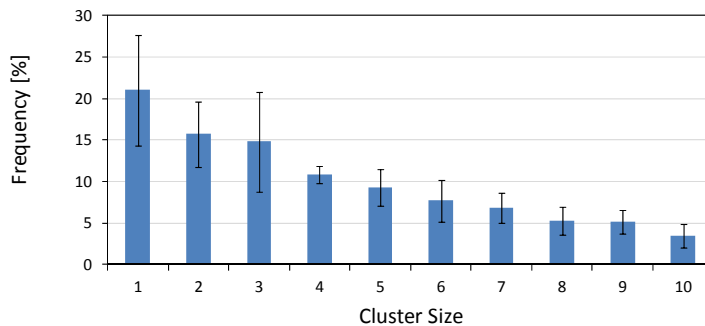

Fig. 6. Individual cluster size distribution averages at r/R=0 radial position

Thus, as shown in Fig. 5 the cluster size distributions found in this study are consistently asymmetric, with smaller particle clusters being the most dominant with this trend being independent of the radial position. It is our view that these typical cluster size distributions are of great importance for the fluid dynamic simulation and design of downer reactors for industrial applications.

4. CONCLUSIONS

(a) A signal baseline reference factor n was established using solid phase mass balances. It was found that the n factor was strongly affected by the mass flux.
(b) Particle cluster size distributions show that particle clusters display asymmetric distributions with smaller particle clusters being the most dominant. This finding was true for all operating conditions and various radial positions considered.

5. ACKNOWLEDGMENT

6. NOTATION

A	Downer internal area, (m^2)
d	Distance between upper and lower focal sensor regions, (m)
d_p	Particle diameter, (m)
G_s	Solid mass flux, $(kg/m^2 \cdot s)$
h	Transversal dimension of the sensing region, (m)
n	Baseline reference factor, (-)
N	Number of particles in a cluster
u_s	Terminal particle velocity, (m/s)
u_{sg}	Superficial gas velocity, (m/s)
u_{slip}	Slip velocity, (m/s)
X	Signal average, (V)
ε_s	Time average solid concentration, (-)
ρ_p	Particle density, (kg/m^3)
σ	Standard deviation, (V)
Δt_i	Sensor signal time length, (s)
τ	Time shift between signals, (s)

7. REFERENCES

(1) J.X. Zhu, Z.Q. Yu, Y. Jin, J.R. Grace, A. Issangya, Cocurrent downflow circulating fluidized bed (downer) reactors – a state of the art review, Can. J. Chem. Eng. 73 (1995) 662–677.
(2) Z. Wang, D. Bai, Y. Jin, Hydrodynamics of cocurrent downflow circulating fluidized bed (CDCFB), Powder Technol. 70 (1992) 271–275.
(3) M.A. Islam, S. Krol, H. de Lasa, Slip velocity in downer reactors: drag coefficient and the influence of operational variables, Ind. Eng. Chem. Res. 49 (2010) 6735–6744.
(4) S.R. Nova, S. Krol, H.I. de Lasa, Radial Distribution of Particle Clusters in Down Flow Reactors, Fluidization XII 108 (2007) 879–888.
(5) S. Nova, S. Krol, H. de Lasa, Particle velocity and particle clustering in down-flow reactors, Powder Technol. 148 (2004) 172–185.
(6) S. Nova, S. Krol, H. de Lasa, CREC Fiber-Optic Probes for Particle Velocity and Particle Clustering: Design Principles and Calibration Procedures, Ind. Eng. Chem. Res. (2004), 43, 5620 – 5631.
(7) A. Lanza, M.A. Islam, H. de Lasa, Particle clusters and drag coefficients in gas–solid downer units, Chemical Engineering Journal 200–202 (2012) 439–451.
(8) S.V. Manyele, J.X. Zhu, H. Zhang, Characterizing cluster dynamics in co-current downflow CFB using optical fiber probe, CIESC J. 61 (2010) 1753–1769.
(9) C.H. Soong, K. Tuzla, J.C. Chen, Identification of particle clusters in circulating fluidized beds, in: A.A. Avidan (Ed.), Circulating Fluidized Bed, Technology IV, Engineering Foundation, New York, (1993), pp. 615–620.
(10) A.K. Sharma, K. Tuzla, J. Matsen, J.C. Chen, Parametric effects of particle size and gas velocity on cluster characteristic in fast fluidized beds, Powder Technol. 111 (2000) 114–122.
(11) S. Krol, A. Pekediz, H. de Lasa, Particle clustering in down flow reactors, Powder Technol. 108 (2000) 6–20.
(12) X.B. Qi, H. Zhang, J. Zhu, Solids concentration in the fully developed region of circulating fluidized bed downers, Powder Technol. 183 (2008) 417–425.